

**Spurious four-wave mixing processes in
generalized nonlinear Schrödinger equations**

Fenja Severing, Uwe Bandelow, Shalva Amiranashvili

submitted: November 30, 2022

Weierstrass Institute
Mohrenstr. 39
10117 Berlin
Germany
E-Mail: fenja.severing@wias-berlin.de
uwe.bandelow@wias-berlin.de
shalva.amiranashvili@wias-berlin.de

No. 2975
Berlin 2022



2020 *Mathematics Subject Classification.* 78A40, 78A60, 91G60.

Key words and phrases. Nonlinear fibers, numerical analysis, modulation instability (MI), four-wave mixing (FWM), nonlinear Schrödinger equation (NLSE), generalized nonlinear Schrödinger equation (GNLSE), split-step Fourier method (SSFM), supercontinuum generation.

Edited by
Weierstraß-Institut für Angewandte Analysis und Stochastik (WIAS)
Leibniz-Institut im Forschungsverbund Berlin e. V.
Mohrenstraße 39
10117 Berlin
Germany

Fax: +49 30 20372-303
E-Mail: preprint@wias-berlin.de
World Wide Web: <http://www.wias-berlin.de/>

Spurious four-wave mixing processes in generalized nonlinear Schrödinger equations

Fenja Severing, Uwe Bandelow, Shalva Amiranashvili

Abstract

Numerical solutions of a nonlinear Schrödinger equation, e.g., for pulses in optical fibers, may suffer from the spurious four-wave mixing processes. We study how these nonphysical resonances appear in solutions of a much more stiff generalized nonlinear Schrödinger equation with an arbitrary dispersion operator and determine the necessary restrictions on temporal and spatial resolution of a numerical scheme. The restrictions are especially important to meet when an envelope equation is applied in a wide spectral window, e.g., to describe supercontinuum generation, in which case the appearance of the numerical instabilities can occur unnoticed.

1 Introduction

Resonant interaction of waves in nonlinear wave systems followed by the emergence of new frequencies, is an important field of nonlinear science [1]. A well-known example of this phenomenon is modulation instability (MI) [2]. It is amazing how many nonlinear waves in totally different systems experience the same spontaneous growth of small modulations as described mathematically with just one nonlinear Schrödinger equation (NLSE) [3–10]. In the long run, MI contributes to the formation of solitons [11], generation of turbulent wave states [12], such as optical supercontinuum [13, 14], formation of spontaneous extreme waves [15–17], etc. Moreover, NLSE is completely solvable [18].

This paper deals with the numerical aspects of MI. Namely, studies of small wave modulations are so fundamentally simple, that it is usually possible to perform them directly for the numerical schemes, which are used to solve NLSE, such as the split-step Fourier method (SSFM) [19–22]. A requirement that the numerical solution reproduces MI, while avoiding nonphysical numerical instabilities, provides information on the applicability of the method [19, 23, 24].

To fix notations, we consider a guided system like an optical fiber, where a harmonic wave (which is proportional to $e^{i(kz-\omega t)}$ and possesses a certain radial structure) is subject to the dispersion relation $k = \beta(\omega)$. To describe a wave packet $\Psi e^{i(\beta_0 z - \omega_0 t)}$ with a slowly varying complex amplitude Ψ and central frequency ω_0 , the dispersion relation is reduced to a set of the dispersion parameters β_j such that

$$\beta(\omega_0 + \nu) \approx \sum_{j=0}^J \frac{\beta_j}{j!} \nu^j = \beta_0 + \beta_1 \nu + D(\nu), \quad (1)$$

where $\beta_{0,1,2}$ are the carrier wave-vector, group delay, and group velocity dispersion (GVD) respectively. We have already introduced the notation $D(\nu)$, which will be useful later on.

The envelope is given by $\Psi = \Psi(z, \tau)$, where $\tau = t - \beta_1 z$ is the time-delay variable, it is governed by the equation

$$i\partial_z \Psi + \frac{\beta_2}{2} (i\partial_\tau)^2 \Psi + \gamma |\Psi|^2 \Psi = 0, \quad (2)$$

which is NLSE in optical notations [25]. Parameter γ accumulates contribution of the (cubic) nonlinear medium response for a quasi-monochromatic wave-packet.

Equation (2) is somewhat special, informally speaking, it accepts $\Psi(0, \tau)$ and returns $\Psi(z, \tau)$, i.e., it is space propagated. Mathematically, however, there is no difference with the time-propagated NLSE appearing in other systems. Also the numerical values of β_2 and γ can be arbitrary, only the sign of $\beta_2\gamma$ counts. An accurate derivation of Eq. (2) requires use of the slowly varying envelope approximation and elimination of the radial degrees of freedom [25].

The simplest solution to Eq. (2)

$$\Psi_{\text{pump}} = \sqrt{P_0} e^{i\gamma P_0 z}, \quad P_0 = \text{const} > 0, \quad (3)$$

describes a constant-amplitude carrier (pump) wave. It is unstable with respect to modulations if $\beta_2\gamma < 0$ (Lighthill criterion, [26]). The key result for what follows reads:

If NLSE (2) is solved numerically using SSFM with the temporal resolution $\Delta\tau$ and evolution step h , the condition

$$h < \frac{2(\Delta\tau)^2}{\pi|\beta_2|}. \quad (4)$$

is needed to correctly reproduce MI [23].

The condition $h < C(\Delta\tau)^2$ is expected for the pseudospectral NLSE solvers, where the discrete Fourier transform turns Eq. (2) into a system of coupled ODEs addressed by, e.g., one of the Runge–Kutta methods [27,28]. The value of C depends on the method and ensures that the numerical ODE solution is stable even for the largest discrete frequency $\propto (\Delta\tau)^{-2}$.

Inequality (4) follows from a direct analytic study of MI within SSFM. Violation of Eq. (4) results in additional spurious instability domains for any $\beta_2\gamma$. After a proper scaling and possible exchange of space and time variables, inequality (4) can be used for other systems experiencing MI, but only as long as NLSE applies. The point is that an accurate description of a specific wave system may require modifications of the standard NLSE, e.g., in the form of Dysthe equation for water waves or generalized nonlinear Schrödinger equation (GNLSE) for optical fibers [25] such that the limitation (4) may become insufficient.

In what follows, we consider the optical GNLSE and generalize Eq. (4). For now, we ignore both the radial effects [29] and dispersion of the nonlinearity [30], i.e., we concentrate on numerical instabilities caused by a general linear dispersion law (1). The following fiber-specific aspects will be taken into account:

(A). GNLSE accounts for several (e.g., $J = 10$) dispersion coefficients in terms of the dispersion operator \hat{D} , where

$$i\partial_z \Psi + \hat{D}\Psi + \gamma|\Psi|^2\Psi = 0, \quad \hat{D} = \sum_{j=2}^J \frac{\beta_j}{j!} (i\partial_\tau)^j, \quad (5)$$

cf. Eq. (2). In return, GNLSE does not require the slowly varying envelope approximation [31–33]. However, the change to a general polynomial dispersion requires a more restrictive condition than Eq. (4).

(B). GNLSE is not necessarily associated with a single pump wave, it perfectly describes a sequence of wave packets with considerably different carrier frequencies, in which case ω_0 is just a suitable reference frequency within the total spectrum [34]. It is then natural to require that the numerical

instabilities do not appear for all involved wave-packets. By doing so, we will see that certain waves cannot be properly described, no matter how small is \hbar .

(C). Last but not least, inequality (4) was derived for the simplest Lie-Trotter splitting, whereas more involved splittings are often used in practical calculations. We will then extend the analysis for an arbitrary splitting. As we will see, more involved schemes do not help much in avoiding the numerical instabilities.

The paper is organized as follows. We briefly revisit MI theory in the context of GNLSE and then study to which extent the true MI is properly reproduced by SSFM, first for the simplest Lie-Trotter splitting. In this way we derive the generalized criterion (4). It turns out, that certain numerical instabilities cannot be avoided by the decrease of \hbar . To address this problem, one needs to apply a proper spectral filter before imposing any restrictions on \hbar . We give examples and summarize by discussing how to deal with all these numerical instabilities in a situation, where MI leads to a considerable spectral broadening. The theory is extended to an arbitrary SSFM in Appendix.

2 Modulation instability

To fix notations we assume that $\gamma > 0$. The GNLSE (5) is then focusing if $\beta_2 < 0$ and defocusing if $\beta_2 > 0$, it is centered at the zero-dispersion frequency if β_2 vanishes in which case MI depends on β_4 . Recall that ω_0 is just a reference (circular) frequency at which GNLSE coefficients are known, other frequencies are counted from ω_0 . Pump frequency is ν , frequencies of the blue- and red-shifted satellite waves will be denoted by $\omega_b = \nu + \Omega$ and $\omega_r = \nu - \Omega$.

It is convenient to replace Ψ by $\psi e^{i\gamma P_0 z}$, such that Eq. (5) takes the form

$$i\partial_z \psi + \hat{D}\psi + \gamma(|\psi|^2 - P_0)\psi = 0. \quad (6)$$

A general (i.e., frequency-shifted) pump-wave is described by $\psi = \sqrt{P_0} e^{iD(\nu)z - i\nu\tau}$, it reduces to Eq. (3) for $\nu = 0$. A perturbed pump wave will be taken in the form

$$\psi = (\sqrt{P_0} + \delta\psi) e^{iD(\nu)z - i\nu\tau},$$

it yields a linear equation involving both $\delta\psi$ and $\delta\psi^*$. The equation can be addressed by the two-color Ansatz,

$$\delta\psi = u(z) e^{-i\Omega\tau} + v^*(z) e^{i\Omega\tau}, \quad (7)$$

which yields two coupled ODEs

$$\begin{aligned} i\partial_z u + \left(D(\nu + \Omega) - D(\nu) \right) u + \gamma P_0 (u + v) &= 0, \\ i\partial_z v + \left(D(\nu) - D(\nu - \Omega) \right) v - \gamma P_0 (u + v) &= 0. \end{aligned} \quad (8)$$

We introduce notations

$$\begin{aligned} N_\nu(\Omega) &= \frac{D(\nu + \Omega) - D(\nu - \Omega)}{2}, \\ M_\nu(\Omega) &= \frac{D(\nu + \Omega) + D(\nu - \Omega)}{2} - D(\nu), \end{aligned} \quad (9)$$

and write ODEs (8) in the matrix form

$$\partial_z \begin{pmatrix} u \\ v \end{pmatrix} = i \left(N_\nu(\Omega) \mathbf{I} + M_\nu(\Omega) \mathbf{J} + \gamma P_0 \mathbf{K} \right) \begin{pmatrix} u \\ v \end{pmatrix}, \quad (10)$$

where

$$\mathbf{I} = \begin{pmatrix} 1 & 0 \\ 0 & 1 \end{pmatrix}, \quad \mathbf{J} = \begin{pmatrix} 1 & 0 \\ 0 & -1 \end{pmatrix}, \quad \mathbf{K} = \begin{pmatrix} 1 & 1 \\ -1 & -1 \end{pmatrix}.$$

The general solution of the system (10) reads

$$\begin{aligned} \begin{pmatrix} u_z \\ v_z \end{pmatrix} &= e^{iz} \begin{pmatrix} N_\nu(\Omega)\mathbf{I} + M_\nu(\Omega)\mathbf{J} + \gamma P_0\mathbf{K} \end{pmatrix} \begin{pmatrix} u_0 \\ v_0 \end{pmatrix} \\ &= e^{izN_\nu(\Omega)} e^{iz} \begin{pmatrix} M_\nu(\Omega)\mathbf{J} + \gamma P_0\mathbf{K} \end{pmatrix} \begin{pmatrix} u_0 \\ v_0 \end{pmatrix}, \end{aligned} \quad (11)$$

where $u(z), v(z)$ are replaced by u_z, v_z for brevity.

In order to compare Eq. (11) with the SSFM results, we reformulate it for one evolution step h

$$\begin{pmatrix} u_{z+h} \\ v_{z+h} \end{pmatrix} = e^{ihN_\nu(\Omega)} e^{ihM_\nu(\Omega)\mathbf{J} + ih\gamma P_0\mathbf{K}} \begin{pmatrix} u_z \\ v_z \end{pmatrix}. \quad (12)$$

The first factor in Eq. (12) does not affect stability. The second (matrix) factor has determinant of 1, such that instability develops if $|\text{Tr}(e^{ihM_\nu(\Omega)\mathbf{J} + ih\gamma P_0\mathbf{K}})| > 2$, which yields

$$\left| \cos\left(h\sqrt{M_\nu(\Omega)(M_\nu(\Omega) + 2\gamma P_0)}\right) \right| > 1. \quad (13)$$

The radicand should then be negative, which is a general MI condition. Since we have agreed that $\gamma > 0$, the instability develops if

$$-2\gamma P_0 < M_\nu(\Omega) < 0. \quad (14)$$

Given the pump frequency ν , Eq. (14) defines the possible unstable intervals on Ω -axis.

Fixing ν and taking $P_0 \rightarrow 0$, we see that all unstable intervals shrink into points (resonant frequencies) at which $M_\nu(\Omega)$ vanishes. One such frequency always exists because $M_\nu(0) = 0$, it corresponds to the classical MI [25, 26, 29, 30]. Others can appear in dispersion-flattened fibers in which case one deals with the so-called four-wave-mixing (FWM) instability [35–39]. Existence of the resonance frequencies is necessary but not sufficient, the sufficient conditions ensure that $M_\nu(\Omega)$ takes negative values in the vicinity of resonances [40]. The classical MI develops if $\beta_2 < 0$.

Now we will figure out to which extent equations (13) and (14) are reproduced by SSFM, first for the simplest Lie-Trotter splitting and then for a general one.

3 Lie-Trotter splitting

Solving Eq. (6) by the Lie-Trotter splitting, one advances from $\psi(z, \tau)$ to $\psi(z + h, \tau)$ in two steps. For definiteness, we will always start with the non-dispersive nonlinear step followed by the dispersive linear step. So, in the first step, ψ is advanced using just $i\partial_z\psi + \gamma(|\psi|^2 - P_0)\psi = 0$. The result provides an initial condition for the second step, which employs $i\partial_z\psi + \hat{D}\psi = 0$. For the case at hand, one can apply this procedure directly to Eq. (10), where we have

$$\begin{pmatrix} u_{z+h} \\ v_{z+h} \end{pmatrix} = e^{ih\gamma P_0\mathbf{K}} \begin{pmatrix} u_z \\ v_z \end{pmatrix},$$

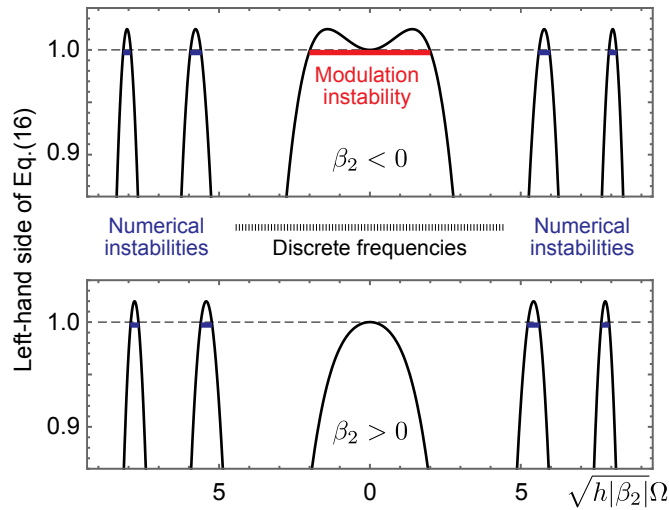


Figure 1: Inequality (16) is illustrated for the NLSE dispersion with $\nu = 0$ and $h\gamma P_0 = 0.2$. MI exists for $\beta_2 < 0$ (top), but not for $\beta_2 > 0$ (bottom). Numerical instabilities are present anyway, to avoid them one can fix the numerical spectral window and reduce h , in which case the unwanted peaks move away from the origin. This is how Eq. (4) appears.

for the non-dispersive part of the GNLSE and

$$\begin{pmatrix} u_{z+h} \\ v_{z+h} \end{pmatrix} = e^{ih \begin{pmatrix} N_\nu(\Omega) \mathbf{I} + M_\nu(\Omega) \mathbf{J} \end{pmatrix}} \begin{pmatrix} u_z \\ v_z \end{pmatrix},$$

for the dispersive part. Therefore, Lie-Trotter's approximation to the exact relation (12) reads

$$\begin{pmatrix} u_{z+h} \\ v_{z+h} \end{pmatrix} = e^{ihN_\nu(\Omega)} e^{ihM_\nu(\Omega)\mathbf{J}} e^{ih\gamma P_0\mathbf{K}} \begin{pmatrix} u_z \\ v_z \end{pmatrix}, \quad (15)$$

and the difference with Eq. (12) arises from the fact that \mathbf{J} and \mathbf{K} do not commute.

Equation (15) can be investigated by analogy with (12). The first factor does not affect stability, both matrix factors have determinant of 1, such that the instability condition is $|\text{Tr}(e^{ihM_\nu(\Omega)\mathbf{J}} e^{ih\gamma P_0\mathbf{K}})| > 2$. The condition is reduced to

$$\left| \cos(hM_\nu(\Omega)) - h\gamma P_0 \sin(hM_\nu(\Omega)) \right| > 1, \quad (16)$$

which is Lie-Trotter's approximation to the exact Eq. (13).

In all practically relevant cases, h is much smaller than the characteristic nonlinear length $(\gamma P_0)^{-1}$ and Eq. (16) contains a dimensionless power parameter $h\gamma P_0 \ll 1$. With respect to the phase parameter $hM_\nu(\Omega)$, we have a harmonic oscillation with the amplitude $\sqrt{1 + (h\gamma P_0)^2}$. Unstable domains always exist, they are localized where $hM_\nu(\Omega) \in \pi\mathbb{Z}$. Specifically, solutions of Eq. (16) for $\gamma > 0$ are given by

$$\pi n - 2 \arctan(h\gamma P_0) < hM_\nu(\Omega) < \pi n, \quad n \in \mathbb{Z}, \quad (17)$$

where the exact MI condition (14) is recovered for $n = 0$.

The point is that $hM_\nu(\Omega)$ is not necessarily small for a given small $h\gamma P_0$, because ν and Ω are arbitrary and limited only by the applicability of GNLSE, which is a very weak restriction [31–33]. Solutions of Eq. (17) with $n \neq 0$ may come into play and yield instabilities with no physical counterpart,

the spurious FWM instabilities (Fig. 1). The latter manifest itself as growing high-frequency oscillations on top of the carrier wave [19, 23], they can be confused with the true FWM instabilities, showing a similar behavior [35–39].

Inequality (4) is necessary to avoid the nonphysical instabilities for the simplest NLSE dispersion and $\nu = 0$. Let us now discuss what to do in a general case. It turns out that the change from NLSE to GNLSE is relatively straightforward, whereas a correct description of the pump waves with $\nu \neq 0$ is much more involved.

4 Filtering

A natural way to eliminate the spurious instabilities is to employ a filter. For now, the filter is just arbitrary, later on it will be related to the numerical discretization. So, we introduce a limiting circular frequency $\bar{\omega}$, define the temporal resolution $\Delta\tau$ such that

$$\bar{\omega} \cdot \Delta\tau = 2\pi, \quad (18)$$

and impose the restriction

$$\omega \in \left[-\frac{1}{2}\bar{\omega}, \frac{1}{2}\bar{\omega}\right], \quad (19)$$

upon all circular frequencies. Given $\bar{\omega}$, it turns out that all nonphysical solutions of Eq. (16) are avoided for a sufficiently small h .

Indeed, Eq. (17) indicates that the numerical instabilities from Section 3 are avoided if $-\pi < hM_\nu(\Omega) < \pi - 2h\gamma P_0$. Performing a similar calculation for $\gamma < 0$, we get the second requirement $-\pi + 2h|\gamma|P_0 < hM_\nu(\Omega) < \pi$. The sufficient condition reads then

$$h|M_\nu(\Omega)| < \pi - 2h|\gamma|P_0,$$

and it should be satisfied on the domain (19). By changing to the satellite frequencies $\omega_b = \nu + \Omega$ and $\omega_r = \nu - \Omega$, we obtain the following statement:

If a GNLSE with the dispersion function $D(\nu)$ is solved with the temporal resolution $\Delta\tau$, calculate the quantity

$$\|D\| = \max_{|\omega_{b,r}| < \frac{\pi}{\Delta\tau}} \left| \frac{D(\omega_b) + D(\omega_r)}{2} - D\left(\frac{\omega_b + \omega_r}{2}\right) \right|.$$

The evolution step h shall obey the inequality

$$h < \frac{\pi}{\|D\| + 2|\gamma|P_0}, \quad (20)$$

where P_0 is a characteristic power of the waves in question.

An evident inequality

$$\max_{|\Omega| < \frac{\pi}{\Delta\tau}} \left| \frac{D(\Omega) + D(-\Omega)}{2} \right| \leq \|D\|,$$

shows that it is insufficient to consider only the “main” pump with $\nu = 0$, as in criterion (4), this results in a too optimistic limitation on h . For instance, by a proper dispersion manipulation one can create a

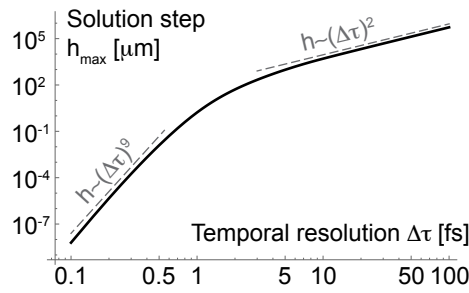


Figure 2: Criterion (20) in the form $h_{\max} = \pi/\|D\|$ is illustrated for a tenth-order $D(\nu)$. The dispersion coefficients are borrowed from [34].

fiber where just one higher-order coefficient $\beta_J \neq 0$, e.g., for $J = 10$, see [41]. In this case Eq. (20) yields

$$\|D\| = C_J \frac{|\beta_J|(\bar{\omega}/2)^J}{J!}, \quad \begin{cases} C_{2n} = 1, \\ C_{2n+1} = \frac{1}{2}(1 - 3^{-2n}), \end{cases}$$

with the scaling $h \propto (\Delta\tau)^J$. The result for an even J is a simple generalization of Eq. (4), whereas the result for an odd J can be derived only by considering pumps with $\nu \neq 0$.

Next, consider a GNLSE in the vicinity of a zero-dispersion frequency by taking $D(\nu) = \frac{1}{2}\beta_2\nu^2 + \frac{1}{6}\beta_3\nu^3$, where the smallness of β_2 necessitates the use of the cubic term, e.g., for studies on Cherenkov radiation [42]. A little more involved calculation yields

$$\|D\| = \begin{cases} \frac{1}{8}|\beta_2|\bar{\omega}^2 & \text{for } \bar{\omega} < 4|\beta_2/\beta_3|, \\ \frac{2}{27}|\beta_3|(\frac{1}{2}\bar{\omega} + |\beta_2/\beta_3|)^3 & \text{for } \bar{\omega} > 4|\beta_2/\beta_3|. \end{cases}$$

We see how the scaling $h \propto (\Delta\tau)^2$, which is predicted by Eq. (4), is replaced by $h \propto (\Delta\tau)^3$ with the increase of the spectral window. It is an undesirable scenario, even more so when $D(\nu)$ is approximated by a higher-order polynomial, as illustrated in Fig. 2 for a tenth-order approximation to a real dispersion law.

A reasonable strategy for a numerical solution is to remain in the domain where $h \propto (\Delta\tau)^2$, e.g., to use $\Delta\tau \gtrsim 3$ fs for the dispersion law from Fig. 2. If a better resolution is necessary, a polynomial approximation of $D(\nu)$ should be replaced by the full dispersion law. If the latter is not available, a rational approximation to $D(\nu)$ should be used [43].

However, this is not the full story. As we will see in the next Section, Eq. (16) and criterion (20) does not cover all spurious FWM instabilities. The remaining ones cannot be defeated by the decrease of h . One should reduce $\Delta\tau$ before choosing h but even so the spurious instabilities cannot be eliminated completely.

5 Time-discretization effect

Solving GNLSE by SSFM, we impose a periodicity condition $\psi(\tau, z) = \psi(\tau + T, z)$ for a sufficiently large T and are left with the discrete frequencies $\omega_n = (2\pi/T)n$ for $n \in \mathbb{Z}$. The interval $[0, T]$ is then uniformly divided by $N + 1$ points with, so to speak, the first-same-as-last property. The temporal resolution reads $\Delta\tau = T/N$, it defines $\bar{\omega} = \omega_N = 2\pi/\Delta\tau$ in accord with Eq. (18).

Note that $e^{-i\bar{\omega}\tau} = 1$ for all discrete τ . Two harmonic oscillations are then indistinguishable if their difference frequency is a multiply of $\bar{\omega}$. All discrete frequencies are automatically projected onto the interval $[0, \bar{\omega}]$, again, with the first-same-as-last property. Note that the second half of the interval $[0, \bar{\omega}]$ (and $[0, T]$) can be interpreted as a container for negative frequencies (and times). We then shift both intervals to the more convenient base ones $[-\frac{1}{2}\bar{\omega}, \frac{1}{2}\bar{\omega}]$ and $[-\frac{1}{2}T, \frac{1}{2}T]$.

To proceed, we have to revisit the MI theory and to take the imposed periodicity into account. The dispersion operator in Eq. (5) changes as follows

$$\hat{D}e^{-i\omega\tau} = D(\{\omega\})e^{-i\omega\tau},$$

where $\{\omega\}$ refers to the projection of ω onto the base interval. The new dispersion function is periodic because by construction $\{\omega + \bar{\omega}\} = \{\omega\}$. Ansatz (7) takes the form

$$\delta\psi = u(z)e^{-i\Omega_b\tau} + v^*(z)e^{-i\Omega_r\tau}, \quad (21)$$

$$\Omega_b + \Omega_r = 0 \pmod{\bar{\omega}}, \quad (22)$$

and the quantities $N_\nu(\Omega)$, $M_\nu(\Omega)$ from Eq. (9) should be replaced by

$$N_\nu(\Omega_b, \Omega_r) = \frac{D(\{\nu + \Omega_b\}) - D(\{\nu + \Omega_r\})}{2},$$

$$M_\nu(\Omega_b, \Omega_r) = \frac{D(\{\nu + \Omega_b\}) + D(\{\nu + \Omega_r\})}{2} - D(\{\nu\}).$$

Finally, the continuous Eq. (14) is now approximated by

$$-2\gamma P_0 < M_\nu(\Omega_b, \Omega_r) < 0, \quad (23)$$

and the Lie-Trotter MI condition (16) becomes

$$\left| \cos(hM_\nu(\Omega_b, \Omega_r)) - h\gamma P_0 \sin(hM_\nu(\Omega_b, \Omega_r)) \right| > 1. \quad (24)$$

Both Eq. (23) and (24) assume that the sideband frequencies are constrained by Eq. (22).

The resulting hierarchy of the MI conditions is summarized as follows:

continuous	Eq. (14)	$h \rightarrow 0$	$\Omega_b + \Omega_r = 0,$
z -discrete	Eq. (16)	$h \neq 0$	$\Omega_b + \Omega_r = 0,$
τ -discrete	Eq. (23)	$h \rightarrow 0$	$\Omega_b + \Omega_r = 0 \pmod{\bar{\omega}},$
z, τ -discrete	Eq. (24)	$h \neq 0$	$\Omega_b + \Omega_r = 0 \pmod{\bar{\omega}}.$

Equation (24) is the main one to compare with Eq. (14), because both z and τ are discrete in a numerical solution. As long as $\Omega_b + \Omega_r = 0$ and solutions of (24) solve (14), they describe the true MI. In addition, Eq. (24) contains spurious instabilities of two types. One is due to the discrete z and appears already in Eq. (16), as described in the Section 4. Another is due to the discrete τ and appears already in Eq. (23), it comes from the solutions with $\Omega_b + \Omega_r = \pm\bar{\omega}$.

Both Eq. (23) and (24) can be simplified considerably. It is natural to assume that the input pump frequency belongs to the interval (19), such that $\{\nu\}$ is replaced by ν . If both $\omega_{b,r} = \nu + \Omega_{b,r}$ belong to the interval (19) as well, Eq. (23) reduces to Eq. (14). If it is not the case, we replace ω_r, ω_b by $\omega_r + \bar{\omega}$ and $\omega_b - \bar{\omega}$. The procedure is repeated until at least one of the satellite frequencies does not fall into the interval (19). We denote the frequency by ω . The other frequency, $2\nu - \omega$, is either

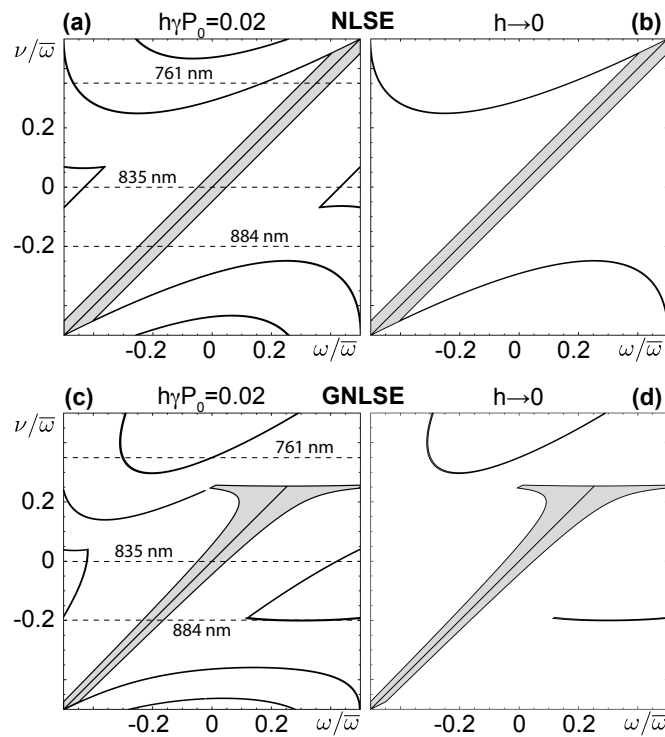


Figure 3: Solutions of Eqs. (23–24) are shown for two sample dispersion laws using Eq. (25). We take NLSE (GNLSE) with β_2 (all β coefficients) from [34] and a pump wave with $\gamma P_0 = 2.75 \text{ m}^{-1}$. In all examples the x axis is centered at 835 nm and covers the frequency band of 100 THz ($\Delta\tau = 2\pi/\bar{\omega} = 10 \text{ fs}$). Frequency offset of the pump is shown on the y axis. For a given ν (dashed lines) one looks for the instability intervals. Intersections of the dashed lines with the thick gray domains describe the true MI, in agreement with Eq. (14). The other instabilities are spurious. Decrease of h removes some but not all of them. The remaining ones are related to spurious FWM processes with $\Omega_b + \Omega_r = \pm\bar{\omega}$. They are always present but can be shifted from the frequency band of interest by reducing $\Delta\tau$.

inside or outside the interval (19) such that we have to keep $\{2\nu - \omega\}$. Altogether, one can make a replacement

$$M_\nu(\Omega_b, \Omega_r) \mapsto \frac{D(\omega) + D(\{2\nu - \Omega\})}{2} - D(\nu), \quad (25)$$

in both Eq. (23) and (24). Their solutions can be plotted as domains on (ω, ν) plane, it is sufficient to plot them inside the square $|\omega|, |\nu| < \frac{1}{2}\bar{\omega}$.

Two typical examples are shown in Fig. 3. The left column shows solutions of Eq. (24), they should be compared to the solutions of Eq. (23), for which $h \rightarrow 0$, in the right column. The gray domains solve both discrete equations as well as the continuous Eq. (14), they describe the true MI.

In contrast with the Section 4, certain spurious instabilities survive even for $h \rightarrow 0$. They are related to the discrete Fourier transform, such behavior is known both for optical fibers [44] and for other systems [45].

To conclude, SSFM automatically induces a spectral filter, however, the outside frequencies are not truly eliminated, they are rather projected onto the base interval (19). Such behavior is a common feature of all discrete systems with a periodic arrangement (e.g., crystals), yet in our case it is artificial and yields spurious instabilities.

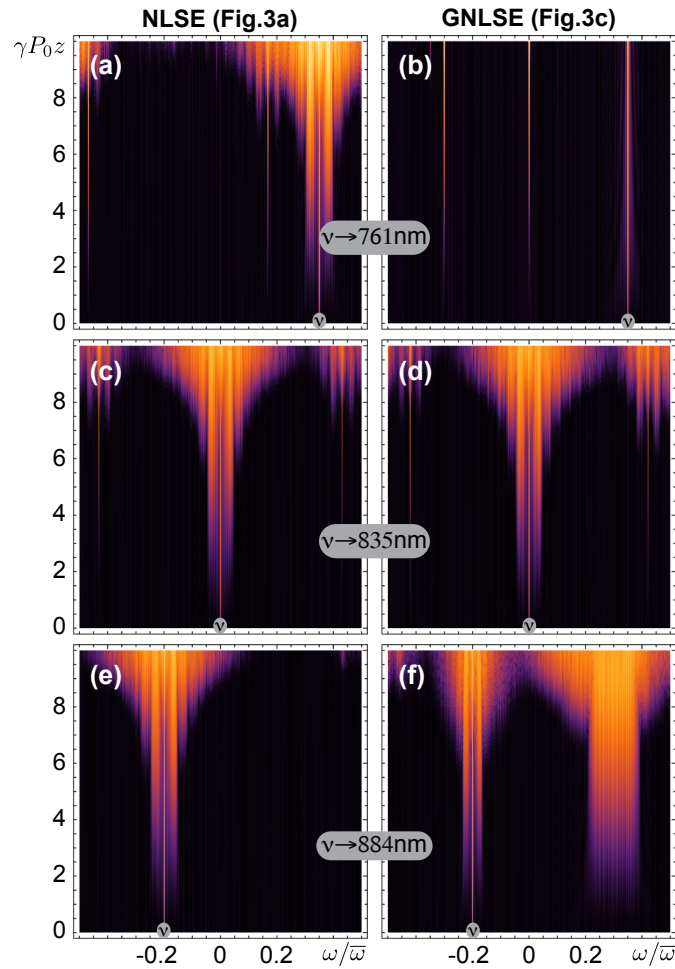


Figure 4: Spurious four-wave mixing is illustrated using the split-step solutions of NLSE (left column) and GNLSE (right column) for three pump waves (gray boxes, $P_0 = 25$ W). Log-plots of the spectral density are shown, the x -axis shows the discrete frequencies [Eq. (19) with $\Delta\tau = 10$ fs], the y -axis shows the propagation length. The GNLSE refers to a nonlinear fiber with $\gamma = 0.11 \text{ W}^{-1}\text{m}^{-1}$. It is centered at 835 nm, β -coefficients are taken from [34]. NLSE accounts only for β_2 , otherwise using the same parameters. Both equations are solved with $h = 0.02/(\gamma P_0)$. The spurious resonances in the left (right) column are as predicted by Fig. 3a (Fig. 3c).

For instance, the GNLSE from Fig. 3d (i.e., even in the ideal case of $h \rightarrow 0$) properly describes the possible pump waves only as long as $|\nu| < 0.2\bar{\omega}$. If it is not enough, one should decrease the temporal resolution $\Delta\tau$. Thereafter one should apply Eq. (20) to determine the largest h .

Spurious instabilities that are predicted by Fig. 3, are illustrated by SSFM solutions of NLSE and GNLSE in Fig. 4. The pump frequency for Fig. 4a,b is chosen such that the spurious satellites are on one side of the pump. This happens because the blue-shifted satellite appears outside the base interval (18) and is therefore represented by its projection. Such situation requires decrease of $\Delta\tau$. Fig. 4c,d describes spurious instabilities that disappear after a proper decrease of h . The pump wave in Fig. 4e accidentally gets into a gap with no spurious resonances. However, the latter reappear for a slightly different value of ν . Finally, Fig. 4d demonstrates simultaneous excitation of numerous spurious resonances, again, from one side of the pump. In all cases the numerical artifacts are properly predicted by the solutions of Eq. (24), as shown in Fig. 3a,c.

6 Conclusions

How should one proceed with a numerical solution of a GNLSE, given the information reported above? One needs a clear idea of the spectral interval of interest. This might be tricky, especially in a turbulent situation when new spectral components are constantly arising, experiencing MI and taking part in other nonlinear interactions. The temporal resolution $\Delta\tau$ should be sufficiently small such that the spurious resonances shown in Fig. 3b,d do not appear for the frequency offsets of interest. That is, the numerical spectral interval should be at the very least two times larger than the one we would like to investigate. Having $\Delta\tau$, one applies Eq. (20) to get the largest possible solution step h , preferably in a domain where $h \propto (\Delta\tau)^2$, see Fig. 2. Finally, one should correctly execute the nonlinear step, which at the very least requires that $h\gamma P_0 \ll 1$, see discussion in [20].

One more point should be mentioned. It is broadly accepted that a properly “long” GNLSE, one that additionally accounts for the Raman self-scattering and includes the shock derivative, applies to nearly any pulse, e.g., to a single-cycle one. This point of view is supported by the perfect agreement between the GNLSE solutions and numerical solutions of the full wave equation [31–33]. Quite naturally, the input pulse frequency of these calculations coincides with the reference frequency of the GNLSE. As for pulses with a considerable frequency offset, e.g., resulting from nonlinear interactions, applicability of the GNLSE might be an issue. This problem needs further research.

Appendix

In this Appendix we generalize the results of Section 3 for an arbitrary splitting scheme. Recall that we agreed to start with the non-dispersive nonlinear step followed by the dispersive linear step. A generic splitting is determined by a set of constants $a_{1 \leq s \leq S}$ and $b_{1 \leq s \leq S}$, where S is the number of stages and $\sum_s a_s = \sum_s b_s = 1$. Equation (6) is written as

$$i\partial_z\psi + \sum_{s=1}^S \left(b_s \hat{D}\psi + a_s \gamma (|\psi|^2 - P_0)\psi \right) = 0.$$

One advances from $\psi(z, \tau)$ to $\psi(z + h, \tau)$ in $2S$ steps, two steps per stage. In the the first stage the nonlinear step is performed using $i\partial_z\psi + a_1\gamma(|\psi|^2 - P_0)\psi = 0$. The result provides the initial condition for the linear step which employs $i\partial_z\psi + b_1\hat{D}\psi = 0$. We get the initial condition for the second stage, the procedure is repeated with a_2 and b_2 , and so on. A proper choice of the splitting coefficients increases accuracy of the approximation, see [46] for a rich collection of known splittings.

Studying MI with a generic splitting, it is easy to see that Eq. (15) takes the form

$$\begin{pmatrix} u_{z+h} \\ v_{z+h} \end{pmatrix} = e^{ihN_\nu(\Omega)} \prod_s e^{ib_s h M_\nu(\Omega) \mathbf{J}} e^{ia_s h \gamma P_0 \mathbf{K}} \begin{pmatrix} u_z \\ v_z \end{pmatrix},$$

where the product runs over $S \geq s \geq 1$ from left to right. Stability of the pump wave is determined by the matrix

$$\begin{aligned} \mathfrak{M} &= e^{y_S \mathbf{J}} e^{x_S \mathbf{K}} e^{y_{S-1} \mathbf{J}} e^{x_{S-1} \mathbf{K}} \dots e^{y_1 \mathbf{J}} e^{x_1 \mathbf{K}}, \\ x_s &= ia_s h \gamma P_0, \quad y_s = ib_s h M_\nu(\Omega). \end{aligned}$$

In a full analogy with Section 3, we have $\det \mathfrak{M} = 1$ and the instability condition is $|\text{Tr} \mathfrak{M}| > 2$. Calculation of the trace is simplified by the fact that $\mathbf{K}^2 = 0$, i.e., one can easily expand $\text{Tr}(\mathfrak{M})$ with

respect to $x_1 \dots x_S$

$$\mathfrak{M} = \mathfrak{M}_0 + \mathfrak{M}_1 + \mathfrak{M}_2 + \mathfrak{M}_3 + \dots,$$

where

$$\begin{aligned}\mathfrak{M}_0 &= e^{y_1^S \mathbf{J}}, \\ \mathfrak{M}_1 &= \sum_p x_p e^{y_p^S \mathbf{J}} \mathbf{K} e^{y_1^{p-1} \mathbf{J}}, \\ \mathfrak{M}_2 &= \sum_{p>q} x_p x_q e^{y_p^S \mathbf{J}} \mathbf{K} e^{y_q^{p-1} \mathbf{J}} \mathbf{K} e^{y_1^{q-1} \mathbf{J}}, \\ \mathfrak{M}_3 &= \sum_{p>q>r} x_p x_q x_r e^{y_p^S \mathbf{J}} \mathbf{K} e^{y_q^{p-1} \mathbf{J}} \mathbf{K} e^{y_r^{q-1} \mathbf{J}} \mathbf{K} e^{y_1^{r-1} \mathbf{J}},\end{aligned}$$

etc. Here y_q^p denotes $y_p + y_{p-1} + \dots + y_q$ and all indices in the above sums run from S to 1.

Note that $\mathfrak{M}_n = O(h\gamma P_0)^n$. One can calculate that Eq. (16) is replaced by

$$\left| \cos(hM_\nu(\Omega)) - \varepsilon \sin(hM_\nu(\Omega)) + O(\varepsilon^2) \right| > 1,$$

where $\varepsilon = h\gamma P_0 \ll 1$ for any reasonable numerical solution of the GNLS. We conclude that the spurious FWM resonances, e.g., those shown in Fig. 1, are practically unaffected by the use of a more advanced splitting method. This general result is confirmed by the direct calculation for a four-stage Yoshida splitting applied to NLSE, see [19].

References

- [1] E. Kartashova. *Nonlinear Resonance Analysis*. Cambridge University Press, 2010.
- [2] V. E. Zakharov and L. A. Ostrovsky. Modulation instability: the beginning. *Physica D: Nonlinear Phenomena*, 238(5):540–548, March 2009.
- [3] T. B. Benjamin and J. E. Feir. The disintegration of wave trains on deep water Part 1. Theory. *J. Fluid Mech.*, 27(3):417–430, February 1967.
- [4] V. I. Karpman. Self-modulation of nonlinear plane waves in dispersive media. *JETP Lett.*, 6(8):277–279, 1967.
- [5] V. E. Zakharov. Stability of periodic waves of finite amplitude on the surface of a deep fluid. *J. Appl. Mech. and Tech. Phys.*, 9(2):190–194, 1968.
- [6] L. A. Ostrovskii. Propagation of wave packets and space-time self-focusing in a nonlinear medium. *JETP*, 24(4):797–800, April 1967.
- [7] A. Hasegawa. Theory and computer experiment on self-trapping instability of plasma cyclotron waves. *Phys. Fluids*, 15(5):870–881, 1972.
- [8] K. Tai, A. Hasegawa, and A. Tomita. Observation of modulational instability in optical fibers. *Phys. Rev. Lett.*, 56(2):135–138, January 1986.
- [9] A. Chabchoub, B. Kibler, C. Finot, G. Millot, M. Onorato, J. M. Dudley, and A. V. Babanin. The nonlinear Schrödinger equation and the propagation of weakly nonlinear waves in optical fibers and on the water surface. *Annals of Physics*, 361:490–500, October 2015.
- [10] K. G. Makris, Z. H. Musslimani, D. N. Christodoulides, and S. Rotter. Constant-intensity waves and their modulation instability in non-Hermitian potentials. *Nat Commun*, 6(7257):1–7, July 2015.
- [11] A. Gelash, D. Agafontsev, V. Zakharov, G. El, S. Randoux, and P. Suret. Bound state soliton gas dynamics underlying the spontaneous modulational instability. *Phys. Rev. Lett.*, 123(23):234102, December 2019.
- [12] V. E. Zakharov, V. S. L'vov, and G. Falkovich. *Kolmogorov spectra of turbulence 1. Wave turbulence*. Springer, Berlin, 1992.
- [13] A. Demircan and U. Bandelow. Analysis of the interplay between soliton fission and modulation instability in supercontinuum generation. *Appl. Phys. B*, 86(1):31–39, 2007.
- [14] J. M. Dudley, G. Genty, F. Dias, B. Kibler, and N. Akhmediev. Modulation instability, Akhmediev breathers and continuous wave supercontinuum generation. *Opt. Express*, 17(24):21497, November 2009.
- [15] N. N. Akhmediev and V. I. Korneev. Modulation instability and periodic solutions of the nonlinear Schrödinger equation. *Theor. Math. Phys.*, 69(2):1089–1093, 1986.
- [16] B. Kibler, J. Fatome, C. Finot, G. Millot, F. Dias, G. Genty, N. Akhmediev, and J. M. Dudley. The peregrine soliton in nonlinear fibre optics. *Nature Physics*, 6(10):790–795, August 2010.

- [17] M. Erkintalo, K. Hammani, B. Kibler, C. Finot, N. Akhmediev, J. M. Dudley, and G. Genty. Higher-order modulation instability in nonlinear fiber optics. *Phys. Rev. Lett.*, 107(25):253901, Dec 2011.
- [18] V. E. Zakharov and A. B. Shabat. Exact theory of two-dimensional self-focusing and one-dimensional self-modulation of waves in nonlinear media. *Sov. Phys. JETP*, 34(1):62–69, 1972.
- [19] J. Yang. *Nonlinear Waves in Integrable and Nonintegrable Systems*. SIAM, 2010.
- [20] O. V. Sinkin, R. Holzlöhner, J. Zweck, and C. R. Menyuk. Optimization of the split-step Fourier method in modeling optical-fiber communications systems. *J. Lightwave Technol.*, 21(1):61–68, January 2003.
- [21] A. Čiegis, A. Mirinavičius, and M. Radziunas. Comparison of split step solvers for multidimensional Schrödinger problems. *Computational Methods in Applied Mathematics*, 13(2):237–250, April 2013.
- [22] W. van Dijk, T. Vanderwoerd, and S.-J. Prins. Numerical solutions of the time-dependent Schrödinger equation in two dimensions. *Phys. Rev. E*, 95(2):023310, February 2017.
- [23] J. A. C. Weideman and B. M. Herbst. Split-step methods for the solution of the nonlinear Schrödinger equation. *SIAM J. Numer. Anal.*, 23(3):485–507, June 1986.
- [24] T. I. Lakoba. Instability analysis of the split-step Fourier method on the background of a soliton of the nonlinear Schrödinger equation. *Numerical Methods for Partial Differential Equations*, 28(2):641–669, March 2012.
- [25] G. P. Agrawal. *Nonlinear Fiber Optics*. Academic, New York, 4 edition, 2007.
- [26] M. J. Lighthill. Contributions to the theory of waves in non-linear dispersive systems. *IMA Journal of Applied Mathematics*, 1(3):269–306, 1965.
- [27] L.N. Trefethen. *Spectral Methods in MATLAB*. SIAM, Philadelphia, 2000.
- [28] C. Canuto, M. Y. Hussaini, A. Quarteroni, and T. A. Zang. *Spectral methods: Fundamentals in single domains*. Springer, Berlin, 3 edition, 2006.
- [29] P. Béjot, B. Kibler, E. Hertz, B. Lavorel, and O. Faucher. General approach to spatiotemporal modulational instability processes. *Phys. Rev. A*, 83(1):013830, January 2011.
- [30] F. Biancalana and D. V. Skryabin. Vector modulational instabilities in ultra-small core optical fibres. *J. Opt. A: Pure Appl. Opt.*, 6(4):301–306, April 2004.
- [31] T. Brabec and F. Krausz. Nonlinear optical pulse propagation in the single-cycle regime. *Phys. Rev. Lett.*, 78(17):3282–3285, 1997.
- [32] P. Kinsler and G. H. C. New. Few-cycle pulse propagation. *Phys. Rev. A*, 67(2):023813, 2003.
- [33] G. Genty, P. Kinsler, B. Kibler, and J. M. Dudley. Nonlinear envelope equation modeling of sub-cycle dynamics and harmonic generation in nonlinear waveguides. *Opt. Express*, 15(9):5382–5387, 2007.
- [34] J. M. Dudley, G. Genty, and S. Coen. Supercontinuum generation in photonic crystal fiber. *Rev. Mod. Phys.*, 78(4):1135–1184, 2006.

- [35] S. B. Cavalcanti, J. C. Cressoni, H. R. da Cruz, and A. S. Gouveia-Neto. Modulation instability in the region of minimum group-velocity dispersion of single-mode optical fibers via an extended nonlinear Schrödinger equation. *Phys. Rev. A*, 43(11):6162–6165, June 1991.
- [36] F. Kh. Abdullaev, S. A. Darmanyan, S. Bischoff, P. L. Christiansen, and M. P. Sørensen. Modulational instability in optical fibers near the zero dispersion point. *Opt. Commun.*, 108(1–3):60–64, May 1994.
- [37] M. Yu, C. J. McKinstrie, and G. P. Agrawal. Modulational instabilities in dispersion-flattened fibers. *Phys. Rev. E*, 52(1):1072–1080, July 1995.
- [38] S. Pitois and G. Millot. Experimental observation of a new modulational instability spectral window induced by fourth-order dispersion in a normally dispersive single-mode optical fiber. *Opt. Commun.*, 226(1–6):415–422, October 2003.
- [39] J. D. Harvey, R. Leonhardt, S. Coen, G. K. L. Wong, J. C. Knight, W. J. Wadsworth, and P. St. J. Russell. Scalar modulation instability in the normal dispersion regime by use of a photonic crystal fiber. *Opt. Lett.*, 28(22):2225–2227, November 2003.
- [40] Sh. Amiranashvili and E. Tobisch. Extended criterion for the modulation instability. *New J. Phys.*, 21(3):033029, March 2019.
- [41] A.F.J. Runge, Y.L. Qiang, T.J. Alexander, and C.M. De Sterke. Linear pulse propagation with high-order dispersion. *Journal of Optics*, 24(11):115502, October 2022.
- [42] J. M. Soto-Crespo, A. Ankiewicz, N. Devine, and N. Akhmediev. Modulation instability, Cherenkov radiation, and Fermi–Pasta–Ulam recurrence. *J. Opt. Soc. Am. B*, 29(8):1930–1936, August 2012.
- [43] Sh. Amiranashvili, U. Bandelow, and A. Mielke. Padé approximant for refractive index and nonlocal envelope equations. *Opt. Commun.*, 283(3):480–485, February 2010.
- [44] G. Bosco, A. Carena, V. Curri, R. Gaudino, P. Poggiolini, and S. Benedetto. Suppression of spurious tones induced by the split-step method in fiber systems simulation. *IEEE Photonics Technology Letters*, 13(5):489–491, May 2000.
- [45] D. Klindworth, M. Ehrhardt, and T. Koprucki. Discrete transparent boundary conditions for multi-band effective mass approximations. In M. Ehrhardt and T. Koprucki, editors, *Multi-Band Effective Mass Approximations*, volume 94 of *Lecture Notes in Computational Science and Engineering*. Springer, 2014.
- [46] <https://www.asc.tuwien.ac.at/~winfried/splitting/>.